

Saddle-point electrons in proton-impact ionization of H: A classical trajectory study

Gunadya Bandarage* and Robert Parson†

*Joint Institute for Laboratory Astrophysics, University of Colorado
and National Institute of Standards and Technology, Boulder, Colorado 80309-0440*

(Received 22 January 1990)

Ionization in $H(1s)+H^+$ collisions is studied in the relative collision energy range 4.0–25.0 keV by classical trajectory simulations. Improved total ionization cross sections are reported for the collision energies 2.0–10.0 keV. A thorough study of the qualitative dynamics of ionization has been carried out, with emphasis placed on the distinction between “direct-impact” and “saddle-point” mechanisms. A precise criterion for classifying trajectories according to these mechanisms is given, and by analyzing the trajectories in a quasistatic molecular frame it is shown that the distinction is established early in the collision. The development of position and velocity-space correlations in ensembles of trajectories of each type is studied.

I. INTRODUCTION

The profound significance of dynamical correlations for ionization processes that lead to three particles in the final state has been appreciated since the pioneering work of Wannier.¹ Wannier’s derivation of the threshold law for two-electron double escape showed that final-state interactions dominate the ionization dynamics at low energies. The efforts of subsequent investigators^{2–6} have provided a detailed understanding of the qualitative dynamics, as manifested by radial and angular correlations, that lies behind the unusual threshold laws. The resulting picture has been aptly termed “a paradigm of highly correlated motion.” While the original theory deals with two light particles escaping from a heavy one, Klar⁶ has considered general mass and charge combinations. His results imply that the dynamics of electrons released in low-energy proton-impact ionization of atoms will be strongly influenced by correlations.

While Wannier’s work was directed toward a derivation of an asymptotic threshold law, it is clear that the underlying physical mechanisms also operate at higher energies.^{7,8} This point has recently been demonstrated by Olson⁷ in classical trajectory simulations of proton-impact ionization of hydrogen atoms. Olson found that at energies less than 60 keV, a substantial fraction of the ionized electrons emerge with close to half of the projectile velocity. These electrons are caught in the region between the receding nuclei—in the vicinity of the “Wannier saddle”—and their presence shows that the traditional analysis of secondary electron spectra in terms of “charge transfer to the continuum” and “electron capture to the continuum” requires modification at low energies. Independent evidence for this phenomenon was obtained by Winter and Lin⁸ in a quantum-mechanical calculation which included basis functions localized between the nuclei. The importance of the Coulomb saddle point in collisional ionization is also demonstrated by the fact that the adiabatic molecular continuum states, which form an appropriate basis to describe the ionized electron

probability, are centered at the saddle point rather than on the nuclei, even at very large internuclear separations.⁹ Very recently, research in this area has been stimulated by experimental investigations,^{10–12} and accompanying trajectory simulations,^{10,11} of proton-helium and He^{2+} -He collisions. (At the energies involved double ionization is negligible so this is not essentially different from the proton-hydrogen case. In fact the results have been successfully modeled using three-body trajectory calculations and an independent-electron approximation.^{10,11})

While the physical mechanism involved in these systems is the same as that which leads to the Wannier threshold law, one cannot expect that the detailed dynamics associated with the latter persists at these high energies. In particular, threshold ionization is dominated by motion on or near to a two-dimensional submanifold of the phase space. (In the language of modern dynamical systems theory, Wannier isolated a center manifold¹³ and analyzed the linearized dynamics in its neighborhood.) One consequence of this reduction is that threshold electrons are emitted near 0° ; at higher energies, the correlated dynamics takes place in a larger phase space and leads to electron emission at nonzero angles. (To emphasize this distinction, Olson *et al.*¹⁰ have introduced the term “saddle-point mechanism” to be used in place of “Wannier mechanism” for the high-energy correlated dynamics.) While considerable evidence for the importance of the saddle-point mechanism has accumulated, and the experimental manifestations of the phenomenon have been worked out in detail, not much attention has been devoted to unraveling the detailed dynamics of the mechanism. Since this dynamics takes place in a eight-dimensional phase space (taking into account constancy of energy and angular momentum) a complete description must be very complicated. Our purpose in this paper is to elucidate, through numerical experiments, some of the qualitative aspects of the saddle-point dynamics.

The most satisfactory sort of numerical experiment would be based upon numerically exact quantum

mechanics; at the present time, though, such a calculation is beyond our reach. We wish, insofar as is possible, to avoid approximations that would bias the results against correlated dynamics. We have therefore used classical mechanics for all particles. The utility of the classical approximation for problems of this sort is well documented.^{14–16} It has been demonstrated recently¹⁷ that not only highly averaged quantities such as total cross sections, but also resolved double-differential cross sections, can be accurately calculated classically at high energies. In our own work we find that microcanonical classical trajectory simulations give reasonably accurate (within a factor of 2 of quantum calculations) total cross sections at energies as low as 4 keV. Of course this does not imply that the detailed dynamics is correct; tunneling and interference effects must become significant at sufficiently low energies. (It is interesting to note that at threshold, classical mechanics becomes accurate again—Wannier’s original calculation was classical.) An assessment of the validity of the classical approximation can only be based upon direct dynamical comparisons to quantum calculations when such become available; in the meantime, classical calculations may suggest the phenomena to be found in a more accurate theory.

In this paper we make four contributions to this problem. First, we describe technical modifications of the standard classical-trajectory Monte Carlo (CTMC) simulation procedure. These include a simplified sampling procedure and the use of perturbation theory for the asymptotic part of the inward propagation. The latter allows us to carry out simulations at low energies where the length scales involved in the problem become very large. Second, we introduce a precise criterion for distinguishing direct-impact and saddle-point electrons, in terms of a dividing surface in the space of asymptotic final momenta. Third, we develop an appropriate *quasistatic molecular frame* in which to analyze the behavior of individual trajectories. (The reader who is familiar with the use of electron-translation factors in molecular state close coupling calculations may be amused by their reappearance, in a sort of inverse form, in the present context.) With the aid of this frame we are able to trace the distinction between impact and saddle-point trajectories back into the interaction region. Finally, we analyze the development in time of position, momentum, and joint position-momentum correlations in the ensemble. Our largely empirical results will be useful in the construction of a comprehensive theory of such correlations.

II. COMPUTATIONAL PROCEDURE

The classical-trajectory Monte Carlo method^{14,16} involves three stages: (i) choice of initial conditions, (ii) numerical integration of equations of motion, and (iii) categorization of each trajectory as excitation, charge transfer or ionization. When Coulomb potentials are involved, special procedures are required. As our procedure differs somewhat from that used in previous studies, we describe it in some detail below.

In the center-of-mass frame, the motion of a three-body system is described by a set of 12 coupled Hamilton

equations. In standard notation they are

$$\dot{r}_i = \frac{\partial H}{\partial p_i}; \quad \dot{p}_i = -\frac{\partial H}{\partial r_i}, \quad i=1,2,3 \quad (1a)$$

$$\dot{R}_i = \frac{\partial H}{\partial P_i}; \quad \dot{P}_i = -\frac{\partial H}{\partial R_i}, \quad i=1,2,3. \quad (1b)$$

\mathbf{P} and \mathbf{p} are the momenta conjugate to \mathbf{R} and \mathbf{r} . (\mathbf{R} and \mathbf{r} are defined in Fig. 1.) For the three-body Coulomb problem, the Hamiltonian (in a.u.) is

$$H = \frac{p^2}{2m} + \frac{P^2}{2\mu} + \frac{Z_A Z_C}{|\mathbf{r} + C_A \mathbf{R}|} + \frac{Z_B Z_C}{|\mathbf{r} - C_B \mathbf{R}|} + \frac{Z_A Z_B}{R} \quad (2)$$

with

$$C_{A(B)} = \frac{m_{B(A)}}{m_A + m_B}, \quad \mu = \frac{m_A m_B}{m_A + m_B}, \quad (3)$$

$$m = \frac{m_C(m_A + m_B)}{m_A + m_B + m_C}.$$

The first stage involves the specification of the dynamical state of the hydrogen atom and the relative motion of the projectile and the atom at $t \rightarrow -\infty$. In the classical hydrogen atom, the electron is in an elliptic orbit described by Kepler’s equation,¹⁸

$$\alpha = \psi - e \sin \psi. \quad (4)$$

α , ψ , and e are the “mean anomaly,” “eccentric anomaly,” and the eccentricity of the ellipse. They are related to the more familiar dynamical variables (in a.u.) as follows:¹⁸

$$e^2 = 1 + \frac{2U l^2}{M}, \quad M = \frac{m_B m_C}{m_B + m_C}, \quad (5)$$

$$r_B = \frac{e \cos \psi - 1}{2U}, \quad (6)$$

$$p_B^2 = 2M \left[\frac{1}{r_B} + \frac{(1-e^2)}{4U r_B} + U \right]. \quad (7)$$

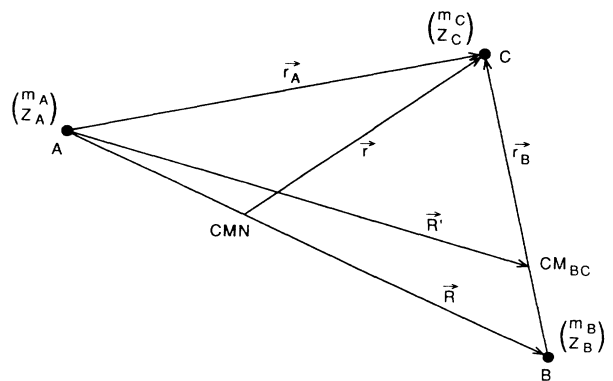


FIG. 1. Definition of various position vectors. A , B , and C are the projectile, target nucleus, and the electron. m_i and Z_i represent the mass and charge of the particle i , respectively.

U is the total energy of the atom, l is the angular momentum, and p_B is the momentum conjugate to r_B . Three angular variables i , Ω , and ω frequently encountered in celestial mechanics problems, which are defined in Fig. 2, are used to specify the orientation of the orbit in space. They are physically transparent and are convenient for studying the possible correlations between the initial orientation of the hydrogenic orbit and the collision products. They also enable easy evaluation of perturbation corrections due to the asymptotic motion of the incoming projectile (Appendix). In terms of these variables, the components of \mathbf{r}_B and $\dot{\mathbf{r}}_B$ are given by

$$r_{B_1} = r_B [\cos\Omega \cos(\omega + \theta) - \sin\Omega \cos i \sin(\omega + \theta)] , \quad (8a)$$

$$r_{B_2} = r_B [\sin\Omega \cos(\omega + \theta) + \cos\Omega \cos i \sin(\omega + \theta)] , \quad (8b)$$

$$r_{B_3} = r_B \sin i \sin(\omega + \theta) , \quad (8c)$$

$$\dot{r}_{B_1} = \frac{1}{Mr_B} \{ p_B r_{B_1} - l [\cos\Omega \sin(\omega + \theta) + \sin\Omega \cos i \cos(\omega + \theta)] \} , \quad (9a)$$

$$\dot{r}_{B_2} = \frac{1}{Mr_B} \{ p_B r_{B_2} - l [\sin\Omega \sin(\omega + \theta) - \cos\Omega \cos i \cos(\omega + \theta)] \} , \quad (9b)$$

$$\dot{r}_{B_3} = \frac{1}{Mr_B} \{ p_B r_{B_3} + l \sin i \cos(\omega + \theta) \} , \quad (9c)$$

where the "true anomaly" θ is given by

$$\tan \frac{\theta}{2} = \left(\frac{1+e}{1-e} \right)^{1/2} \tan \frac{\psi}{2} . \quad (10)$$

We wish to choose these variables from a microcanonical ensemble, with $U = -0.5$ a.u. To achieve this, we choose α and e from a uniform distribution¹⁴ in

$$0 \leq \alpha < \pi, \quad 0 \leq e^2 < 1 . \quad (11)$$

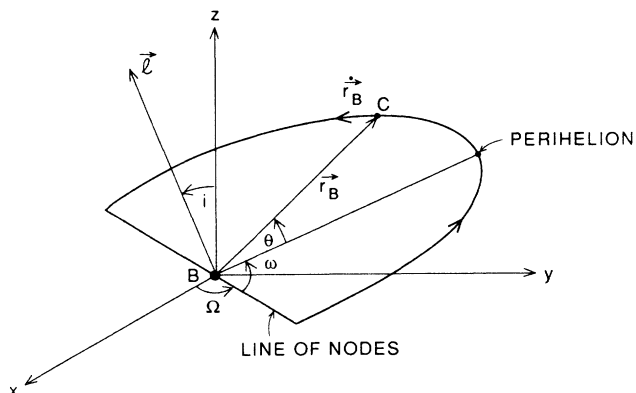


FIG. 2. Definition of the angles i , Ω , and ω . The plane of the orbit intersects the xy plane along the line of nodes.

Isotropy of space dictates that $\cos(i)$, Ω , and ω are uniformly distributed in

$$-1 \leq \cos i \leq +1, \quad 0 \leq \Omega < 2\pi, \quad 0 \leq \omega < 2\pi . \quad (12)$$

The projectile moves in the xz plane along the z axis with a relative velocity dictated by the collision energy. Since the projectile beam is assumed to have a uniform intensity over its cross section, the square of the impact parameter b is uniformly distributed in the range

$$0 \leq b^2 \leq b_{\max}^2 \quad (13)$$

where b_{\max} is the maximum impact parameter beyond which the reaction of interest is negligible. b_{\max} must be determined by numerical experiment. For this purpose we have used curves similar to those shown in Fig. 3, generated by running the CTMC program at constant b . The quantities in Eqs (11)–(13), chosen for each trajectory using six random numbers, along with the relative collision velocity, fully specify the state of the system at $t \rightarrow -\infty$. The second stage involves the numerical integration (we have used a variable-order variable-step Runge-Kutta routine) of the Eqs. (1), in and out of the reaction zone, starting from a sufficiently large internuclear separation so that the calculated cross sections are converged. (The Coulomb singularities at the nuclei poses no significant difficulty since (a) the probability of encountering a highly singular trajectory is very low and (b) the variable step size in the integration routine automatically acts to accurately integrate the near singular trajectories.) At low collision energies one has to begin the integration at very large distances which makes the computations expensive. We have alleviated this by using classical perturbation theory¹⁸ to calculate the changes in the Kepler constants of motion accrued during propagation from infinity to an inner radius, at which numerical integration

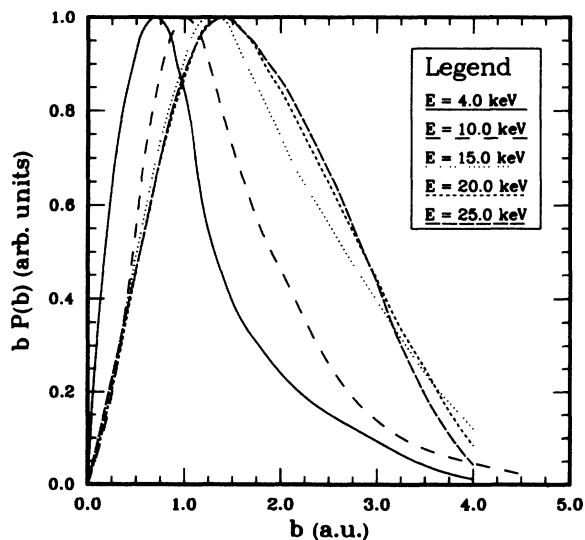


FIG. 3. Opacity as a function of impact parameter at a number of different relative collision energies. Each curve is normalized so that the maximum is equal to unity.

commences. The technique we used to calculate the variations of the components of angular momentum and the Laplace-Runge-Lenz vector is outlined in the appendix.

When the receding nuclei are sufficiently far apart, several tests may be used to characterize the reaction. We have used a criterion similar to that described in Ref. 19. A negative electronic energy in a rest frame of one of the nuclei, disregarding the other, indicates that the electron is bound to the former nucleus. An ionizing trajectory is characterized by the electron not being bound to either of the nuclei and moving away from them. The total ionization cross section is then given by

$$\sigma = 2\pi b_{\max}^2 \frac{N_{\text{ion}}}{N}, \quad (14)$$

where N_{ion} is the number of ionizing trajectories in an ensemble of N trajectories.

III. IONIZATION CROSS SECTIONS

The impact parameter dependence of the classical ionization is depicted in Fig. 3. At each energy, the opacity function $bP(b)$ is normalized so that the peak height is unity. At lower collision energies a larger fraction of ionized electrons are produced by the trajectories with small impact parameters. These curves are qualitatively similar

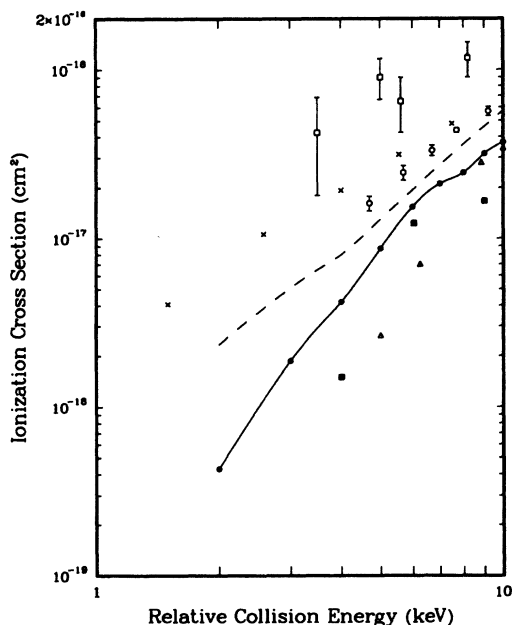


FIG. 4. Total ionization cross section for $H(1s)+H^+$ collisions as a function of relative collision energy: (a) —, present results. The estimated error decreases with increasing collision energy. At 10.0 keV the error bars are of the size of the solid dots. (b) \square , experiment (Ref. 21); (c) \circ , experiment (Ref. 22); (d) — —, AO+ calculation (Ref. 20); (e) \times , triple center calculation (Ref. 8); (f) \triangle , CTMC (Ref. 23); (g) \blacksquare , CTMC (Ref. 24).

to those obtained in quantum mechanical calculations⁸ except that the quantum curves have long tails extending to large impact parameters. However the classical functions cover the range of impact parameters where most of the ionization originates, so the effect of these tails on the cross section is small.

In Fig. 4, we have compared our total ionization cross sections, at low collision energies, with quantum-mechanical close-coupling calculations,^{8,20} experiment^{21,22} and the existing CTMC results.^{23,24} The present results, which have a maximum estimated error of 30% at the lowest collision energy 2.0 keV, are in better agreement with the quantum calculations and with experiment than the previous CTMC calculations. The improvement in our results over the past CTMC results may be due to (a) our accounting for the corrections due to the asymptotic motion of the incoming proton, (b) better statistics, and (c) better coverage of the contributing impact parameters. (As expected, the agreement eventually deteriorates with the decreasing collision energy.) Our results for more energetic collisions agree with the CTMC calculations reported in Ref. 25.

A representative distribution of an ensemble of ionizing trajectories (generated by CTMC method) on the ρz plane when the distance between the receding protons is 100.0 a.u. is shown in Fig. 5. In this figure ρ and z are the two distance components in the familiar cylindrical polar coordinates (in a molecule fixed reference frame). One observes an enhanced density of electrons near $z=0$, where the saddle point of the Coulomb potential created by the two nuclei is located. These electrons may be called the “saddle-point” (SP) electrons. In the rest of this paper we present a characterization of these elec-

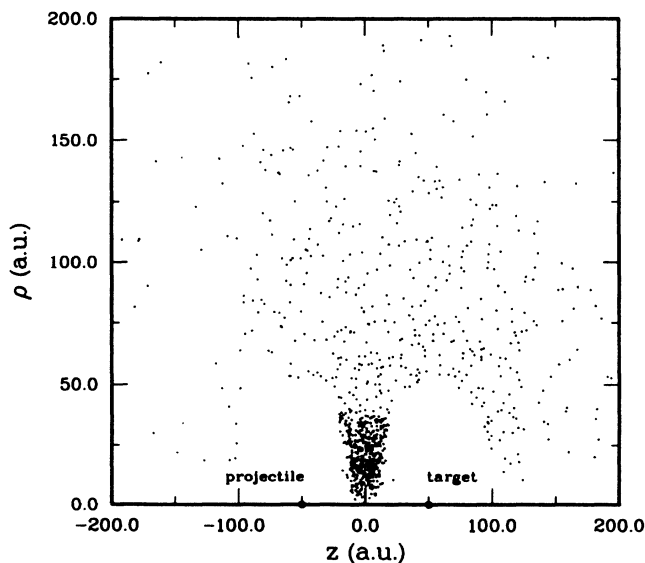


FIG. 5. Distribution of the electronic positions on the ρz plane in an ensemble of 1000 ionizing trajectories when the receding protons are 100 a.u. apart. Relative collision energy equals 4.0 keV.

trons and show that, as an ensemble, they behave differently from the rest which may be called the "direct-impact" (DI) electrons. Our results and observations are generally valid in the relative collision energy range 4.0 to 25.0 keV.

IV. QUASISTATIC MOLECULAR FRAME

Saddle point electrons, because of their spatial location, are equally strongly affected by both nuclei. We therefore analyze our results using a molecule-fixed reference frame in which, at each instant in time, the nuclei are held fixed with respect to laboratory coordinates. We call this the "quasistatic molecular frame." The electronic energy in this frame, which we call the molecular electronic energy, is the classical analog of the Born-Oppenheimer electronic energy. In a collision problem, one must distinguish between the molecular energy and the *total* energy of the electron with respect to the center of mass of the nuclei. The latter quantity, because of its oscillatory nature, is not an easily interpreted quantity. The origin of these oscillations, exemplified in curve *a* of Fig. 6, is easily understood: the moving nuclei "drag" the electron with them which imparts a certain velocity component on it. When freezing the nuclei one must subtract this drag velocity, which creates the oscillatory behavior in total electronic energy, in order to obtain a slowly varying quantity. At $t \rightarrow -\infty$ the drag velocity is equal to the velocity of the target nucleus since the electron is in an atomic bound state of it. However, within the interaction region, where the three particles interact strongly with each other, the magnitude of the drag is not so obvious.

One encounters the same question in close-coupling calculations using molecular basis states.^{26,27} Molecular orbitals do not contain any information about the nuclear motion. One incorporates this information into molecular states using electron translation factors, to obtain dynamic molecular states which provide an appropriate basis for the quasimolecule formed in slow atomic collisions.²⁶ The construction of the proper electron translation factors requires a prior estimate of the drag velocity.

In our classical calculation we are faced with the inverse problem; we have the exact (classical) dynamics in hand, and we wish to represent it in a quasistatic picture. With this proviso, we may adapt the devices used in previous studies. The drag velocity with respect to the center of mass of the nuclei is represented by

$$V_d = f(\mathbf{r}, \mathbf{R}) \dot{\mathbf{R}}. \quad (15)$$

The switching function f for an electron in a bound state has the following asymptotic properties:

$$f(\mathbf{r}, \mathbf{R}) = \begin{cases} f_0(\mathbf{r}, \mathbf{R}) \exp(-\beta r) & \text{if the electron is not bound to any nucleus} \\ f_0(\mathbf{r}, \mathbf{R}) & \text{otherwise.} \end{cases}$$

In our numerical evaluations we have used $\beta=0.01$. This gives converged results for $P_u(t)$ defined below.

We now define the molecular energy of a trajectory at any instant of time by

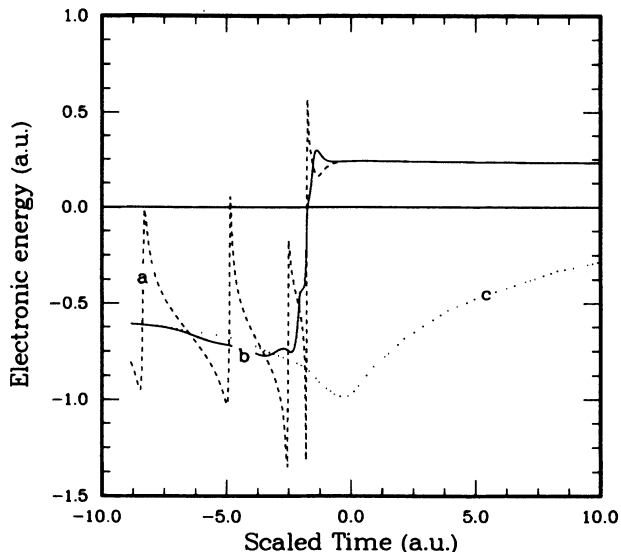


FIG. 6. Time dependence of electronic energy for two particular trajectories. Relative collision energy equals 4.0 keV. Curve *a*, total electronic energy of a DI trajectory in a space-fixed reference frame centered at the center of mass of nuclei. Curve *b*, total electronic energy of the same trajectory in the quasistatic molecular frame. Curve *c*, total electronic energy of an SP trajectory in the quasistatic molecular frame.

$$f(\mathbf{r}, \mathbf{R}) = \begin{cases} -\frac{1}{2} & \text{as } r_B \rightarrow \infty, r_A \text{ finite} \\ +\frac{1}{2} & \text{as } r_A \rightarrow \infty, r_B \text{ finite} \end{cases}, \quad (16)$$

which guarantees that V_d approaches the appropriate nuclear velocity when $R \rightarrow \infty$. Numerous models have been proposed²⁸⁻³⁰ for a functional form of f ; we use the one in Ref. 28. In this model the switching function is independent of a particular molecular state which makes it easy to adapt to our classical calculation. The drag velocity is assumed to be equal to the velocity of the point of intersection of the two vectors \mathbf{R} and the total nuclear force on the electron. The corresponding switching function is given by

$$f_0(\mathbf{r}, \mathbf{R}) = \frac{1}{2} \left[\frac{r_A^3 - r_B^3}{r_A^3 + r_B^3} \right]. \quad (17)$$

A slight modification is necessary to take into account the fact that there cannot be any drag when an ionized electron is far away from the interaction region. We account for this by introducing an exponential decay factor. Our switching function then becomes

$$E_m(t) = \frac{1}{2} m \sum_{i=1}^3 [\dot{r}_i - f(\mathbf{r}, \mathbf{R}) \dot{R}_i]^2 - \frac{1}{r_A} - \frac{1}{r_B}. \quad (18)$$

Note that the decay factor guarantees that E_m asymptoti-

cally approaches the total energy of the ionized electron with respect to the center of mass of the nuclei (which is positive). Curve *b* in Fig. 6 shows that E_m is a much smoother function of time³¹ than the total electronic energy.

V. TRAJECTORY RESULTS

A. Molecular energy of saddle-point versus direct-impact trajectories

In an ensemble of trajectories, two extreme cases of behavior of E_m can be identified. In one case (Fig. 6, curve *b*) the electron is impulsively promoted to a positive energy state, while in the other the (Fig. 6, curve *c*) trajectory spends a long time in the portion of the phase space corresponding to molecular Rydberg states before entering into the subspace of positive energy states. The former type of trajectory produces the *direct impact* electrons and the latter, the *saddle point* electrons.

The *scaled* time depicted in the figures and denoted by T in the text is defined as $T = -vt$, where v is the asymptotic relative nuclear velocity. To a good approximation the nuclei move in straight line paths (although we have not made such an assumption in our CTMC calculations) except at very small impact parameters which make a negligible contribution to the total cross section. Hence for most of the trajectories $T \approx -R_3$. At large t , $T \approx R$ for all the trajectories, and it directly represents the scale of the nuclear subsystem.

To obtain a complete picture of an ionizing event in a real atom, we must consider statistical properties. To this end, we define the probability of population of unbound states $P_u(t)$ by

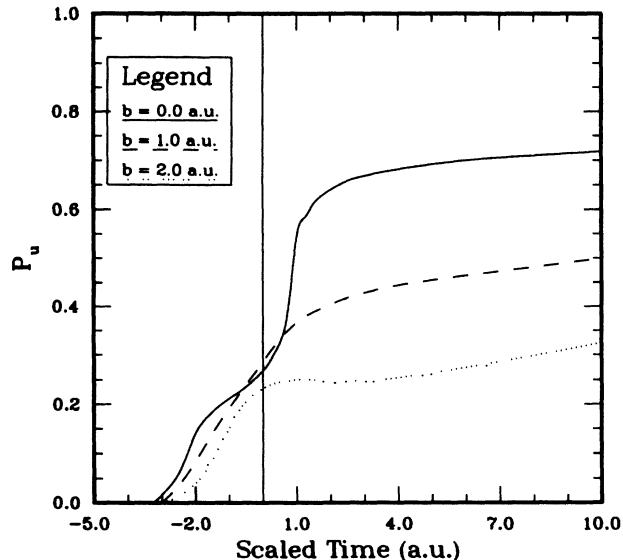


FIG. 8. Time variation of $P_u(t)$ at a number of different impact parameters. Relative collision energy equals 25.0 keV.

$$P_u(t) = N_u(t)/N, \quad (20)$$

where $N_u(t)$ is the number of trajectories whose molecular energy is positive, at time t , in an ensemble of N ionizing trajectories. The asymptotic properties of E_m guarantee that

$$\lim_{t \rightarrow +\infty} P_u(t) = 1. \quad (21)$$

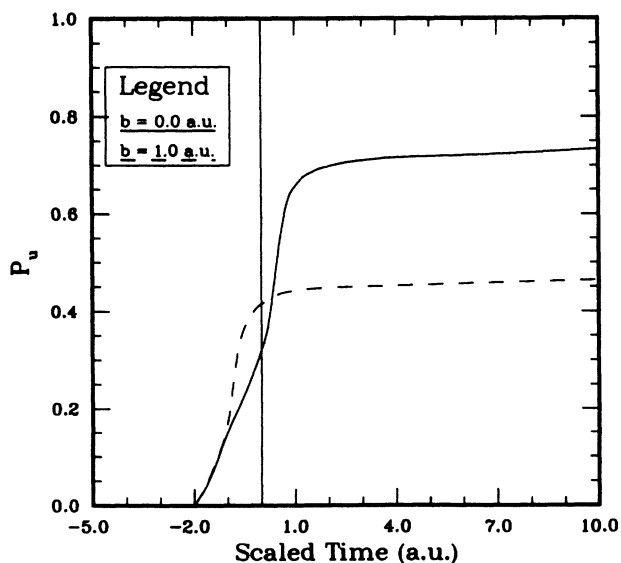


FIG. 7. Time variation of $P_u(t)$ at a number of different impact parameters. Relative collision energy equals 4.0 keV.

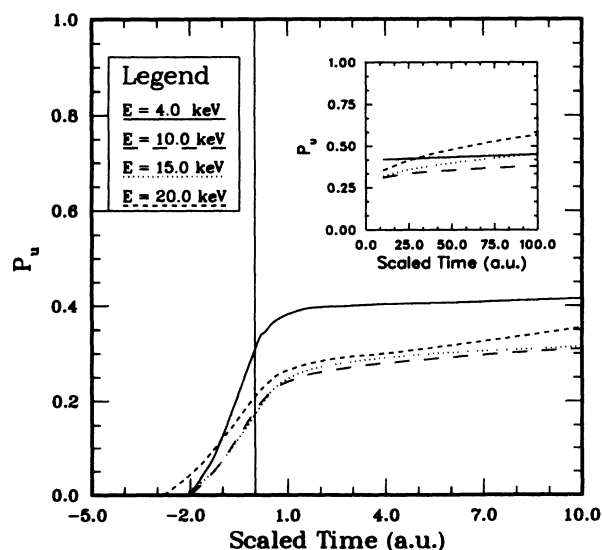


FIG. 9. Time variation of $P_u(t)$ at a number of different collision energies. Inset displays the long-time behavior of $P_u(t)$ at the same collision energies.

With our definition of molecular energy $P_u(t)$ is a smooth function of time which provides insights into the ionization process throughout the collision. Figures 7 and 8 illustrate the typical behavior of $P_u(t)$ at constant impact parameter. To construct each curve, we have used 1000 ionizing trajectories generated by the CTMC method at fixed b . There is a sudden transfer of population into the unbound molecular states around $T=0$ where the nuclei are close to each other but the rise in $P_u(t)$ is slow at later times. The impulsive excitation of the electron is seen to be more efficient at lower impact parameters.

The behavior of $P_u(t)$ in an ensemble of 1000 ionizing trajectories generated by the full CTMC method is illustrated in Fig. 9. Qualitatively these curves are similar to those discussed earlier; but since they have been averaged over b , they provide a more complete picture of the classical ionization process. Close to $T=0$, impulsive excitation is most efficient at lower collision energies. This seemingly counterintuitive behavior has a simple explanation: at lower energies most of the ionizing events are generated by trajectories having small impact parameters, and these tend to produce more direct impact electrons. The intuitive behavior of $P_u(t)$ is recovered at longer times. It is interesting to note that even at $R=100.0$ a.u. ($T=100.0$ a.u.), a large fraction of the ionizing trajectories correspond to molecular bound states.

The rate of excitation to positive molecular states undergoes a drastic change around $T=1-2$ a.u. which suggests a natural definition of the DI and SP trajectories. We regard the subensemble of ionizing trajectories which attains a positive E_m before $T=2.0$ a.u. as direct impact ionization. When analyzed in this way, the trajectory re-

sults are not very sensitive to the exact value of T as long as it is close to 2. The rest of the ionizing trajectories give rise to the SP electrons. Our results for the fraction of SP electrons, i.e., $P_u(T=2.0$ a.u.) as a function of collision energy are presented in Fig. 10. It is evident that, at these energies, only a small fraction of ionization takes place via direct impact trajectories.

B. Dynamical correlations

The dynamics of the SP trajectories is qualitatively different from that of the DI trajectories. The receding protons have a profound influence on the SP electrons. At an intermediate distance, the electrons are focussed along the straight line which bisects the internuclear axis. At zero impact parameter, the motion along this line represents a dynamically unstable equilibrium state and any electron which executes this motion will eventually

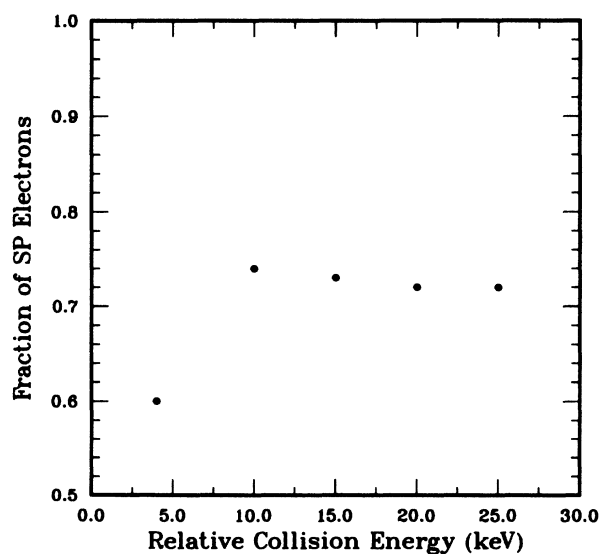


FIG. 10. Probability of SP electron production is displayed as a function of energy. Note that the SP electron production is less efficient at lower collision energies.

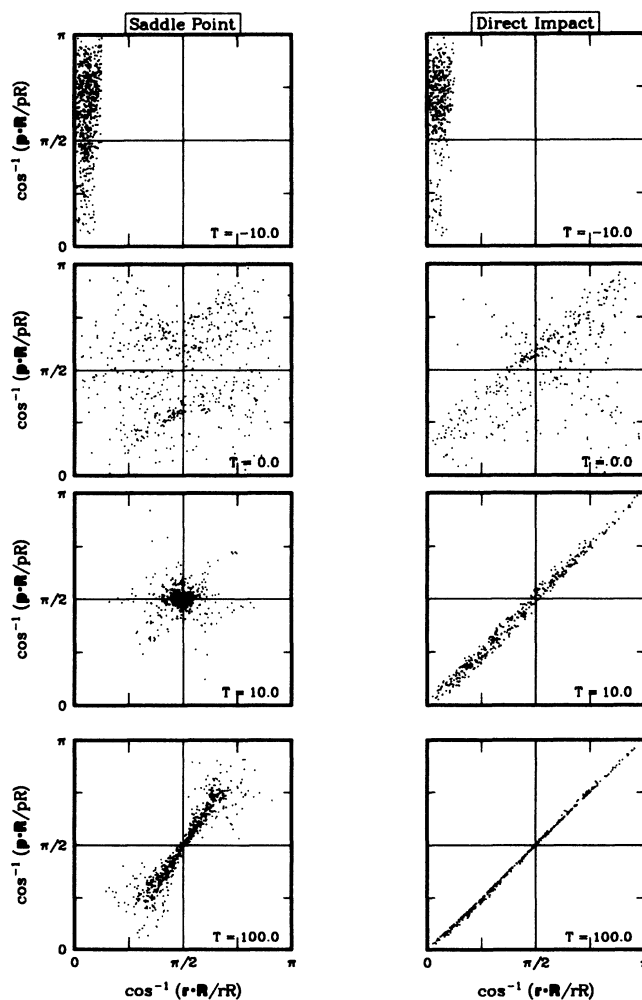


FIG. 11. Distribution of electrons in (θ_r, θ_p) plane at a number of different times. Total of 1000 ionizing trajectories generated by the full CTMC method were used. Relative collision energy = 4.0 keV.

become ionized. Figures 11 and 12 illustrate the strong interplay of the forces acting upon the three particles. We have depicted phase-space distributions of the two different kinds of trajectories by means of a projection onto a plane of two angular coordinates θ_r and θ_p . $\theta_r = \cos^{-1}(\mathbf{r} \cdot \mathbf{R} / rR)$ is the angle between the electronic position vector \mathbf{r} and the internuclear vector \mathbf{R} and $\theta_p = \cos^{-1}(\mathbf{p} \cdot \mathbf{R} / pR)$ is the angle between the electronic momentum vector and \mathbf{R} (See Fig. 13). Note that \mathbf{p} is the momentum conjugate to \mathbf{r} and is independent of any model. When the distance between the receding protons is much greater than the impact parameter, the time variation of (θ_r, θ_p) for a trajectory provides a measure of the degree of correlation. In particular an electron (nearly) free from a nuclear attraction is characterized by an approximately constant θ_p and a θ_r which asymptotically approaches θ_p .

At $T = -10.0$ a.u., the electron has a drag velocity component equal to $-v/2$ since it is in the ground atom-

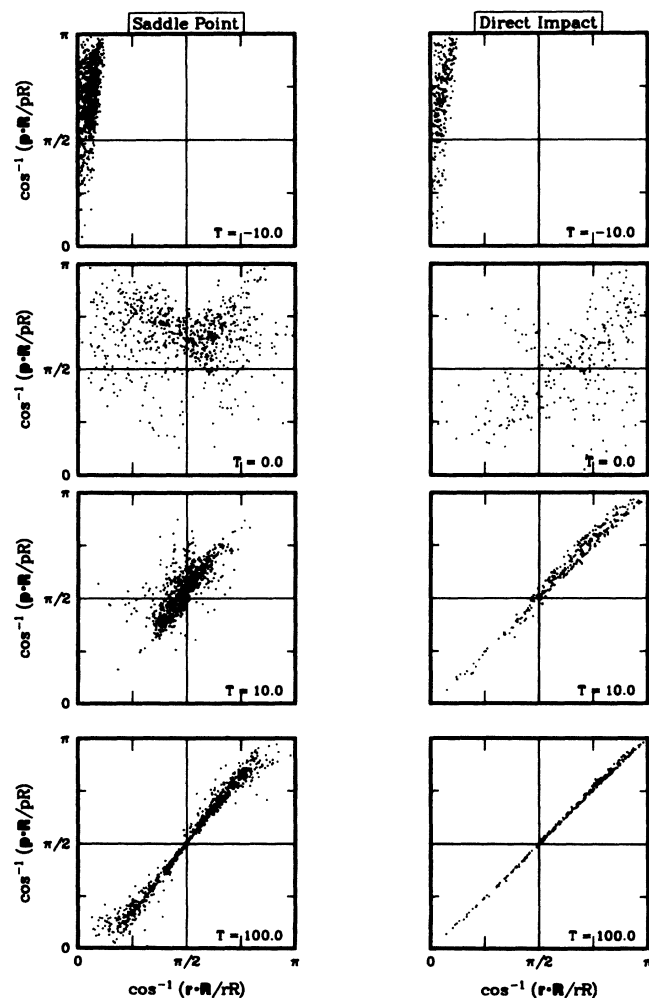


FIG. 12. Distribution of electrons in (θ_r, θ_p) plane at a number of different times. Total of 1000 ionizing trajectories generated by the full CTMC method were used. Relative collision energy = 25.0 keV.

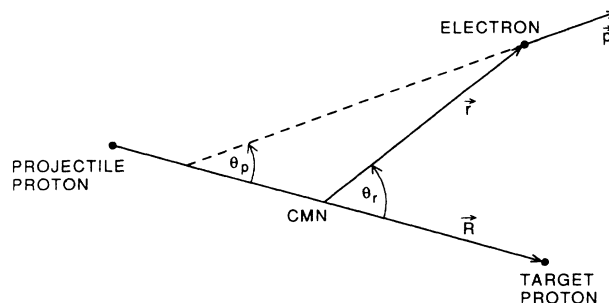


FIG. 13. Definition of the angles θ_r and θ_p for a planar trajectory.

ic state of the target proton; because of this there are more trajectories in the upper left quadrant at this time. At $T=0$ the trajectories are scattered in all four quadrants. In subsequent motion the DI trajectories quickly become asymptotic in the sense that \mathbf{p} become (nearly) parallel to \mathbf{r} while the SP trajectories are focused into the point $(\pi/2, \pi/2)$. As time progresses the electrons move away from the saddle point region and the direction of \mathbf{p} slowly spreads over all possible values.

At lower collision energies more DI trajectories are found in the lower left quadrant but more energetic collisions produce more DI trajectories in the upper right quadrant. This effect is in qualitative agreement with the conventional picture of ionization wherein the electron is impulsively excited into an atomic continuum state of ei-

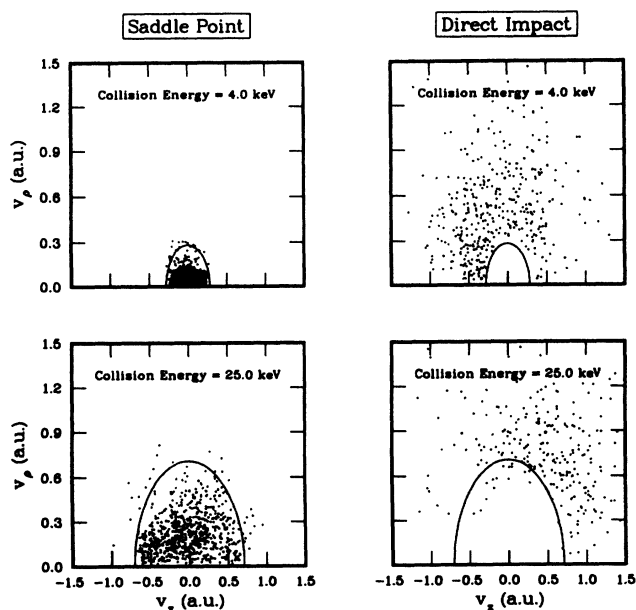


FIG. 14. Asymptotic electronic velocity (relative to CMN) distributions of DI and SP trajectories at two different collision energies. V_ρ and V_z are the velocity components in usual cylindrical polar coordinates.

ther the projectile (electron capture to the continuum) or the target (charge transfer to the continuum) with the latter becoming more important at moderately high energies.³² Such an effect is not very prominent with the SP electrons. This fact is more clearly seen in the ejected electron velocity distributions displayed Fig. 14.

C. An asymptotic definition of saddle-point electrons

Figure 14 was generated by integrating the equations of motion (1) out to $R = 5000$ a.u. and recording the asymptotic values of the velocities $V_\rho \equiv \dot{\rho}$ and $V_z \equiv \dot{z}$ in the usual cylindrical coordinate system centered at center of mass of the nuclei. The figure shows that in the space of asymptotic velocities, DI and SP electrons are separated by the curve

$$(V_\rho^2 + V_z^2)^{1/2} = v/2 \quad (22)$$

where $v/2$ is the proton velocity with respect to center of mass of the nuclei. (There are, as one can see, a few discrepancies at the highest kinetic energy; a small fraction of the trajectories assigned as "saddle point" inside the interaction region end up on the outside of the asymptotic boundary, and vice versa. This probably reflects a certain arbitrariness in any definition of a total energy in a quasistatic molecular frame at such high energies.³¹) Hence, one may define the saddle-point electrons as the ones having an asymptotic speed smaller than that of the protons in the frame of the center of mass of the nuclei. This definition has the advantage that it characterizes the SP electrons with an experimentally measurable quantity and it is straightforward to evaluate the fraction of such electrons using the double differential cross sections. (To our knowledge, no published double-differential cross sections, obtained either from experiment or quantum-mechanical calculations, exist for this system at the energies we studied.)

VI. DISCUSSION

Our contributions to the problem of correlated dynamics in proton-impact ionization have been of two sorts, technical and conceptual. In the first area, we have developed an improved technique for classical-trajectory Monte Carlo simulations of proton-impact ionization. Our use of perturbation theory to correct the long-range propagation have enabled us to obtain accurate total ionization cross sections at low collision energies. We have also found a simple yet precise way to distinguish between "direct-impact" and "saddle-point" ionization trajectories—one simply compares the asymptotic electron velocity to the asymptotic velocity of the receding nuclei. This criterion, based as it is upon experimentally observable quantities, can be directly related to the measured double-differential cross section. It also has a clear quantum-mechanical analog, in terms of the overlap between an outgoing wave packet and the asymptotic states specified by definite values of electron and proton momenta.

We have devoted considerable attention to the qualitative dynamics of individual trajectories and of trajectory

ensembles. By introducing an appropriate definition for the molecular electronic energy, we are able to show that the distinction between impact and saddle-point ionization mechanisms is established very early in the collision. The saddle-point electrons, which make a large contribution to the total ionization cross section even at rather high energies, are strongly influenced by the motion of both nuclei long after the collision has begun. In this respect, they resemble the threshold electrons studied by Wannier. The "Wannier electrons," however, are emitted in the forward direction whereas the classical saddle-point electrons are emitted in all directions, presumably up to a maximum scattering angle of $\pi/2$ in the laboratory frame. The dynamics of the saddle-point electrons at energies well above threshold is considerably more complicated than it is at threshold since it takes place in a larger phase space. Our study of the evolution of position-velocity correlations (Figs. 11 and 12) illustrates this.

Using Wannier's arguments one can see that at threshold all the ionization flux emerges as saddle-point electrons. This fact, along with the results depicted in Fig. 10, implies the existence of a dip in the probability of saddle-point electron production as a function of collision energy. This effect is caused by the delicate dependence of the energy transfer between the electron and the nuclear subsystem, not only on the relative nuclear velocity but also on the impact parameter.

To this point our study has been largely empirical. Many challenging questions emerge from this work, among them the nature of the dividing surface *inside the interaction region* that separates impact and saddle-point trajectories, and the detailed mechanisms behind the position-velocity correlations. Some (though not all) of these issues can be addressed in the context of planar model calculations. Work along these lines is in progress.

ACKNOWLEDGMENTS

This work is supported by National Science Foundation Grant No. PHY86-04504 through the University of Colorado. The graphics and the computations were done on the JILA VAX 8600 and at the CU Academic Computing Services, respectively. We wish to thank Professor C. H. Green and Professor J. S. Briggs for helpful discussions.

APPENDIX

We outline here an approximate semianalytical method to calculate the changes in a Kepler orbit due to the asymptotic motion of the incoming projectile. We use classical time-dependent perturbation theory.

The Hamiltonian of the three-body system can be decomposed into three parts:

$$H = H_{r_B} + H_{R'} + H' , \quad (A1)$$

where H_{r_B} represents the atomic Hamiltonian $P_B^2/2M - 1/r_B$. Free motion of the projectile is represented by $H_{R'}$, $[P_{R'}^2/2\mu'; \mu' = m_A(m_B + m_C)/$

$(m_A + m_B + m_C)$. The perturbation is

$$H' = H_+ + H_- , \quad (\text{A2})$$

$$H_{\pm} = \frac{Z_{\pm}}{|\mathbf{R}' \mp C_{\pm} \mathbf{r}_B|} , \quad (\text{A3})$$

$$C_{+(-)} = \frac{m_{C(B)}}{m_B + m_C} . \quad (\text{A4})$$

The time evolution of any constant of motion K of the Kepler motion is given exactly by

$$\Delta K = \Delta K_+ + \Delta K_- , \quad (\text{A5})$$

$$\Delta K_{\pm} = \int_{-\infty}^t K_{\pm} dt = \int_{-\infty}^t [K, H_{\pm}] dt . \quad (\text{A6})$$

In Eq. (A6), $[]$ represents the Poisson bracket which can be evaluated conveniently in spherical polar coordinates

$$-\frac{\partial H_{\pm}}{\partial r_B} = \pm \frac{C_{\pm} Z_{\pm} x^2 [(b \sin \Theta \cos \Phi \pm C_{\pm} r_B) x - \cos \Theta]}{[(b^2 + C_{\pm}^2 r_B^2 \pm 2C_{\pm} b r_B \sin \Theta \cos \Phi) x^2 \mp 2C_{\pm} r_B \cos \Theta + 1]^{3/2}} . \quad (\text{A9})$$

Similar expressions are obtained for $-\partial H_{\pm}/\partial \Theta$ and $-\partial H_{\pm}/\partial \Phi$. Expansion of the denominator in Taylor series about $x = 0$ gives asymptotic expansions in $-vt$,

$$\begin{aligned} -\frac{\partial H_{\pm}}{\partial r_B} &= \sum_{j=2}^n a_j^{\pm} x^j , & -\frac{\partial H_{\pm}}{\partial \Theta} &= \sum_{j=2}^n b_j^{\pm} x^j , \\ -\frac{\partial H_{\pm}}{\partial \Phi} &= \sum_{j=2}^n c_j^{\pm} x^j . \end{aligned} \quad (\text{A10})$$

By straightforward algebra one can evaluate the first few coefficients a_j^{\pm} , b_j^{\pm} , and c_j^{\pm} . We do not list them here since they are unwieldy. Insertion of these expansions in (A6) gives

$$\Delta K_{\pm} = \sum_{j=2}^n \int_{-\infty}^t A_j^{\pm} x^j dt , \quad (\text{A11})$$

where

$$A_j^{\pm}(r_B, \Theta, \Phi) = \frac{\partial K}{\partial p_B} a_j^{\pm} + \frac{\partial K}{\partial p_{\Theta}} b_j^{\pm} + \frac{\partial K}{\partial p_{\Phi}} c_j^{\pm} , \quad (\text{A12})$$

A_j^{\pm} are periodic functions of time along the path of the unperturbed motion since (r_B, Θ, Φ) describes a point which moves on a Kepler orbit.

When v is much smaller than the typical orbit velocity and the projectile is far away from the target, the change in x over a Kepler period is much smaller than x itself. Hence we can safely replace x in Eq. (A11) by its average over each period which reduces the integral to a summation

$$\Delta K_{\pm} = \sum_{j=2}^n B_j^{\pm} S_j , \quad (\text{A13})$$

(r_B, Θ, Φ) of \mathbf{r}_B and their conjugate momenta ($p_B, p_{\Theta}, p_{\Phi}$). Since H_{\pm} involves only the spatial coordinates, we have

$$K_{\pm} = - \left[\frac{\partial K}{\partial p_B} \frac{\partial H_{\pm}}{\partial r_B} + \frac{\partial K}{\partial p_{\Theta}} \frac{\partial H_{\pm}}{\partial \Theta} + \frac{\partial K}{\partial p_{\Phi}} \frac{\partial H_{\pm}}{\partial \Phi} \right] . \quad (\text{A7})$$

The first-order approximation is obtained by performing the time integral in (A6) over the path of unperturbed motion. Then

$$\mathbf{R}' = b\mathbf{i} + vt\mathbf{k} , \quad (\text{A8})$$

where \mathbf{i} and \mathbf{k} are unit vectors on x and z axes. v is the relative collision velocity. This simplification allows one to express K_{\pm} in an asymptotic expansion in vt . Direct substitution of (A8) with $x = -1/vt$ gives

$$S_j = \sum_{i=1}^{\infty} x_i^j , \quad B_j^{\pm} = \int_0^{2\pi} \frac{1}{\dot{\theta}} A_j^{\pm}(\theta) d\theta . \quad (\text{A14})$$

Note that using the analytical expressions for the Kepler motion one can express A_j^{\pm} solely as a function of the true anomaly θ .

A Kepler orbit is completely characterized by six independent constants of motion. It is convenient to choose these to be the three components of angular momentum l_x, l_y, l_z two components of the Laplace-Runge-Lenze vector, say A_x, A_y , and the initial true anomaly θ_0 . Given the trajectory initializing variables $(E, \alpha, e, i, \Omega, \omega)$ we can easily evaluate the constants. Equations (A13) and (A14) reveal that the asymptotic propagation is done over an (infinite) integral multiple of orbit periods. Under such conditions we have found that the changes in θ_0 are small compared to the perturbations in the other five quantities, except in those few cases where the eccentricity is nearly equal to unity. Hence only the perturbations of the latter five quantities were calculate.

Most of the integrals in the first few coefficients B_j^{\pm} can be done analytically; the rest can be evaluated efficiently by numerical integration. Since B_j^{\pm} are independent of collision energy, they can be stored and used to run trajectories at different collision energies. Once a starting point for the numerical integration of the Hamilton's equations is chosen, S_j can be evaluated to arbitrary accuracy by performing the summations in (A14) numerically. These quantities are independent of the parameters of a particular trajectory; they need to be evaluated one for a given collision energy. Once the perturbed quantities l_x, l_y, l_z, A_x , and A_y are calculated, it is straightforward to evaluate the corrected set of variables $(E, \alpha, e, i, \Omega, \omega)$ which can be used to initialize the trajectory.

*Present address: Department of Chemistry, Texas A&M University, College Station, TX 77843-3255.

†Also at Department of Chemistry and Biochemistry, University of Colorado.

¹G. Wannier, *Phys. Rev.* **90**, 817 (1953).

²R. Peterkop, *J. Phys. B* **4**, 513 (1971).

³A. R. P. Rau, *Phys. Rev. A* **4**, 207 (1971); *Phys. Rep.* **110**, 369 (1984).

⁴U. Fano, *Rep. Prog. Phys.* **46**, 97 (1983).

⁵J. Macek and S. Watanabe, *Comments At. Mol. Phys.* **19**, 313 (1987).

⁶H. Klar, *Z. Phys. A* **307**, 75 (1982).

⁷R. E. Olson, *Phys. Rev. A* **33**, 4397 (1986).

⁸T. G. Winter and C. D. Lin, *Phys. Rev. A* **29**, 3071 (1984).

⁹G. Bandarage and W. R. Thorson, *Phys. Rev. A* **37**, 716 (1988).

¹⁰R. E. Olson, T. J. Gay, H. G. Berry, E. B. Hale, and V. D. Irby, *Phys. Rev. Lett.* **59**, 36 (1987).

¹¹V. D. Irby, T. J. Gay, J. Wm. Edwards, E. B. Hale, M. L. McKenzie, and R. E. Olson, *Phys. Rev. A* **37**, 3612 (1988).

¹²W. Meckbach, P. J. Focke, A. R. Goni, S. Suarez, J. Macek, and M. G. Menendez, *Phys. Rev. Lett.* **57**, 1587 (1986).

¹³J. Guckenheimer and P. Holmes, *Nonlinear Oscillations, Dynamical Systems, and Bifurcations of Vector Fields* (Springer-Verlag, New York, 1983).

¹⁴R. Abrins and C. I. Percival, *Proc. R. Soc. London* **88**, 861 (1966).

¹⁵C. I. Percival and R. Richards, *Adv. At. Mol. Phys.* **11**, 1 (1975).

¹⁶R. E. Olson and A. Salop, *Phys. Rev. A* **16**, 531 (1977); (see Ref. 25 also).

¹⁷C. O. Reinhold and R. E. Olson, *Phys. Rev. A* **39**, 3861 (1989).

¹⁸H. Goldstein, *Classical Mechanics*, 2nd ed. (Addison-Wesley, Reading, MA, 1980).

¹⁹J. S. Cohen, *Phys. Rev. A* **27**, 167 (1983).

²⁰W. Fritsch and C.D. Lin, *Phys. Rev. A* **27**, 3361 (1983).

²¹W. L. Fite, R. F. Stebbings, D. G. Hummer, and R. T. Brackmann, *Phys. Rev.* **119**, 663 (1960).

²²M. B. Shah, D. S. Elliott, and H. B. Gilbody, *J. Phys. B* **20**, 2481 (1987).

²³D. Banks, K. S. Barnes, and J. McB. Wilson, *J. Phys. B* **9**, L141 (1976).

²⁴J. S. Cohen, *J. Phys. B* **18**, 1759 (1985).

²⁵J. S. Cohen, *Phys. Rev. A* **26**, 3008 (1982).

²⁶W. R. Thorson and J. B. Delos, *Phys. Rev. A* **18**, 117 (1978) and references therein.

²⁷G. Bandarage, Ph.D. thesis, University of Alberta, Edmonton, Alberta, Canada (1987).

²⁸J. Vaaben and K. Taulbjerg, *J. Phys. B* **14**, 1815 (1981).

²⁹J. Rankin and W. R. Thorson, *Phys. Rev. A* **18**, 1990 (1978).

³⁰A. Riera, *Phys. Rev. A* **30**, 2304 (1984).

³¹In quantum calculations, a molecular switching function of the form given in Eq. (17) is usually used at low collision energies where the relative nuclear velocity is less than 1 a.u.; this corresponds to a relative collision energy < 12.5 keV. We have used it up to 25.0 keV to smooth the otherwise oscillatory electronic energy. The smoothing is not perfect at higher collision energies. What is more important for our study, though, is the behavior of the function $P_u(t)$ which summarizes the statistical behavior of the trajectories. Our drag removal procedure gives stable smooth curves for $P_u(t)$.

³²B. H. Bransden, *Adv. At. Mol. Phys.* **15**, 263 (1979).